Diverse features of magnetization curves of uniaxial crystals: A simulation study

Hala A. Sobh† and Samy H. Aly

Department of Physics, Faculty of Science at Damietta, Damietta University, P. O. Box 89, *New Damietta* 34517, *Egypt*

(Received 12 June 2016; revised manuscript received 28 June 2016; published online 30 November 2016)

We present a simulation of the magnetization curves, energy, probability, and torque landscapes of uniaxial systems with up to five anisotropy constants. The total energy used in the simulation is the sum of the anisotropy and Zeeman energies. The exchange interaction is not considered in the present work in which we treat single-domain-particle systems within a classical mechanics-based model. Diverse features of the calculated magnetization curves are highlighted for the studied systems. These diverse features are strongly dependent on the sign and magnitude of the simulation parameters. The model is versatile enough to handle both hypothetical and real material systems, e.g. $HoFe_{11}Ti$ and Y_2Co_{17}.

Keywords: magnetization curve, saturation moments, magnetic anisotropy, ferromagnetic metals and alloys

PACS: 75.60.Ej, 75.30.Cr, 75. 30.Gw, 75.50.Cc **DOI:** 10.1088/1674-1056/26/1/017503

1. Introduction

We use the fundamentals of classical statistical mechanics in constructing a model to calculate selected magnetic properties of uniaxial hexagonal and tetragonal systems. In this method, we construct the partition function which is subsequently used to derive physical properties of anisotropic magnetic systems,[1] such as magnetization and the most probable orientations of the magnetization vector for different system parameters.

One of the aims of the present study is to explore the role that the magnetocrystalline anisotropy plays in the magnetization process. This role is expected to result in very different magnetization curves. Some ferromagnetic materials have magnetic anisotropy constants which may span 1–2 orders of magnitude, in addition to the diversity in the temperature dependence of their anisotropy constants.[2,3]

The first attempt, to present an analytical solution for ferromagnetic systems with two anisotropy constants, has been published by de Jesus *et al.*[4] Other researchers reported on analytical works on systems with three anisotropy constants.[5–7] It is hoped that simulating the magnetization curves for more complex systems, i.e. systems described by several (up to five) anisotropy constants, would be beneficial in handling both real and hypothetical systems. For example, unusual or peculiar temperature dependence of anisotropy has been reported by Millev *et al.*,[8,9] Kaczmarek *et al.*,[10] Qian *et al.*,[11] and Opahle *et al.*[12] on hypothetical MCo_5 compounds.

There are different methods for calculating the magnetization curves of magnetically ordered materials. One well-known method is the energy-density minimization method. This method basically depends on finding the magnetization angle at which the system's energy is minimum. Consequently, the field dependence of magnetization is determined by calculating the magnetization component along the field direction. Several authors have used this approach for calculating the magnetization curves.[13–16] In particular, theoretically calculated magnetization curves have been obtained by Johnson *et al.*[14] for magnetic fields applied along different orientations of a ferromagnetic cubic single crystal. Moreover, Kim *et al.*[15] have used the same approach for calculating the magnetization curves of the $Pr_2Fe_{14}B$ compound in the two-sublattice scheme.

Other methods have been reported for calculating the magnetization curves.[17–20] For example, Hatta *et al.*[17] have used the Green's function theory for calculating the magnetization curves of Fe and Ni in high magnetic fields. An application of the hyperbolic model of magnetization has been presented by Meszaros.[18] Using the aforementioned model, Meszaros calculated the normal magnetization curves of soft magnetic iron–nickel and iron–silicon alloys. He concluded that the calculated curves show good consistency with the measured ones for all magnetic fields up to saturation. Furthermore, Zhdanova *et al.*[19] have calculated the magnetization curves for the orthorhombic FeB single crystal along the main crystallographic directions. Their calculations, based on the Neel theory of magnetic phases, showed a good agreement to the experimental curves. Using this approach, they also determined the saturation fields along different principal axes and the magnetocrystalline anisotropy constants.

Moreover, extensive theoretical calculations of the magnetization curves, which took both the crystal and exchange fields into consideration, showed that this method is appropriate for describing the properties of the rare-earth transi-

†Corresponding author. E-mail: hala.amala@gmail.com

© 2017 Chinese Physical Society and IOP Publishing Ltd

tion metal compounds, e.g., $R_2Fe_{14}B$,[21–23] $R_2Co_{14}B$,[24] and $HoFe_{11}Ti$ under the effect of high pressure.[25]

We adopt, in the present method, a dimensionless-parameter approach. This approach takes into account the relative strength of the different anisotropy terms, and the Zeeman energy compared to the thermal energy k_BT of the magnetic systems at thermal equilibrium assuming, of course, that they are in thermodynamic equilibrium. Several normalization options have been reported in the literature to suit the methods used.[6,7,26,27] For example, a normalization to the first anisotropy constant K_1 was used for systems described by only two anisotropy constants.[26] For systems with three constants, however, the choice was to normalize to K_1 [6] or K_3.[7] Our choice of normalizing relative to the thermal energy has the versatility of carrying out the calculation of the magnetization curves without referring to a particular temperature-dependence of the anisotropy constants. In addition, it demonstrates the strong effect that the thermal energy has on the magnetization process of the systems studied. We have successfully applied the method described here to calculate the magnetization curves of compounds of diverse magnetic properties, e.g., $Sm_2Fe_{17}N_x$,[28] $(Nd_{1-x}Pr_x)_2Co_{14}B$ with $x = 0$–1,[29] Y_2Co_{17}, and Gd_2Co_{17}.[30] It is planned to report on those material systems in the near future.

2. Theoretical model and computation

It is known that the magnetic energy of magnetic materials may include different kinds of energies, e.g., magnetocrystalline anisotropy, shape anisotropy, magnetoelastic and magentostrictive anisotropies. Each type of these anisotropies participates differently in the total energy density for different magnetic systems.[31,32]

The total energy of any magnetic system, however, depends on the model used to describe it. In this work, we focus only on the magnetocrystalline anisotropy energy besides the Zeeman energy. Therefore, we adopt the rigid model (a single sublattice) for describing the energy density of the uniaxial magnetic systems under study. We also assume a single-domain particle approach, i.e., no domain wall motion is considered. Therefore, the total energy density can be expressed as follows:[33]

$$E(T,H,\theta_m,\varphi_m) = E_a + E_z, \tag{1}$$

where E_z is the Zeeman energy ($-\boldsymbol{H}\cdot\boldsymbol{M}_s$). In the spherical polar coordinates, it takes the following form:

$$\boldsymbol{H}\cdot\boldsymbol{M}_s = M_sH\left[\sin\theta_m\sin\theta_h\cos(\varphi_m-\varphi_h)+\cos\theta_m\cos\theta_h\right] \tag{2}$$

where subscripts m and h refer to the angular coordinates of the magnetization and the external magnetic field, respectively. The anisotropy energies E_a for hexagonal and tetragonal systems[33,34] are respectively given by

$$E_a = K_1\sin^2\theta_m + K_2\sin^4\theta_m + (K_3+K_4\cos 6\varphi_m)\sin^6\theta_m, \tag{3}$$

$$E_a = K_1\sin^2\theta_m + (K_2+K_3\cos 4\varphi_m)\sin^4\theta_m + (K_4+K_5\cos 4\varphi_m)\sin^6\theta_m. \tag{4}$$

The phenomenological energy expression we are using is suitable for single-domain-particle systems. The magnitude of the saturation magnetization is constant but its direction is dependent on the external field strength and direction. In such a case, no magnetization through domain wall motion is presumed. The very assumption of strictly parallel magnetic moments inside the particle, as a result of a large ferromagnetic exchange interaction, means that this part of the energy is independent of the angular coordinates (θ_m, φ_m) of the magnetization vector.

Therefore including the exchange in the total energy density expression would not affect either a minimization process to calculate $M(H)$,[3,4,14,35–39] or magnetization calculated within the framework of the present work, because calculation of the isothermal magnetization curves from the partition function is done on the magnetization angular coordinates, the exchange interaction is independent of such coordinates. Using this energy expression is not infrequent in the literature, e.g., references [40]–[49] used it for systems with collinear sublattice magnetization[37] for $R_2Fe_{14}B$ system.

Detailed analysis of the inter- and intra-sublattice interactions, and their respective magnetization in an external magnetic field plus their anisotropy energies have been reported by numerous authors.[15,20,33] Therefore, more involved Hamiltonians that take into consideration the exchange and crystal fields have been worked out.[22,23]

Now, multiply both sides of Eqs. (1) and (2) by $V\beta$, and introduce the following dimensionless parameters: $\varepsilon_T = V\beta E(T,H,\theta_m,\varphi_m)$, $\varepsilon_a = V\beta E_a$, $\varepsilon_{zt} = V\beta E_z$, $\alpha = V\beta K_1$, $\gamma = V\beta K_2$, $\delta = V\beta K_3$, $\zeta = V\beta K_4$, $\sigma = V\beta K_5$, $\varepsilon_z = V\beta M_sH$, where V is the volume of a uniformly magnetized spherical particle and $\beta = 1/k_BT$, with k_B being the Boltzmann constant and T the absolute temperature. The total energy densities of the hexagonal and tetragonal systems respectively become

$$\varepsilon_T = \alpha\sin^2\theta_m + \gamma\sin^4\theta_m + (\delta+\zeta\cos 6\varphi_m)\sin^6\theta_m - \varepsilon_z\left[\sin\theta_m\sin\theta_h\cos(\varphi_m-\varphi_h)+\cos\theta_m\cos\theta_h\right], \tag{5}$$

$$\varepsilon_T = \alpha\sin^2\theta_m + (\gamma+\delta\cos 4\varphi_m)\sin^4\theta_m + (\zeta+\sigma\cos 4\varphi_m)\sin^6\theta_m - \varepsilon_z\left[\sin\theta_m\sin\theta_h\cos(\varphi_m-\varphi_h)+\cos\theta_m\cos\theta_h\right]. \tag{6}$$

The classical partition function, in this case, is given by

$$Z(T,H) = \frac{1}{4\pi}\int_0^{2\pi}\int_0^{\pi}\exp(-\varepsilon_T)\sin\theta_m\,\mathrm{d}\theta_m\,\mathrm{d}\varphi_m, \tag{7}$$

where $\varepsilon_{\rm T}$ represents the ratio of the total energy density to the thermal energy. Using this constructed partition function, we can calculate the magnetization and the most probable angular coordinates of the magnetization vector.[1]

The magnetization normalized to the spontaneous magnetization $M_{\rm s}$ and the probability expressed in terms of the dimensionless quantities are given as

$$\frac{M}{M_{\rm s}} = \frac{\partial \ln Z}{\partial \varepsilon_z}, \tag{8}$$

$$P(\varepsilon_z, \theta_m, \varphi_m) = \frac{{\rm e}^{-\varepsilon_{\rm T}}}{Z}. \tag{9}$$

In addition, the three-dimensional (3D) plots of the magnetic energy surface, energy density, and torque landscapes are important for correlating the magnetization curves with these quantities. The torque on the magnetization vector due to the magnetic anisotropy is derived as follows.The torque exerted by an external field on the magnetization vector is given by

$$\boldsymbol{\tau}_{\rm z} = \boldsymbol{m} \times \boldsymbol{H}_{\rm ext}. \tag{10}$$

The effective field due to the anisotropy only ($\varepsilon_z = 0$) can be expressed as[50]

$$\boldsymbol{H}_{\rm eff} = -\nabla_m \varepsilon_{\rm a}, \tag{11}$$

where ∇_m is the gradient with respect to m. Consequently, the torque due to the anisotropy is

$$\boldsymbol{\tau}_{\rm a} = -\boldsymbol{m} \times \nabla_m \varepsilon_{\rm a}. \tag{12}$$

By combining Eqs. (10) and (12), the total torque takes the following form:

$$\boldsymbol{\tau} = \boldsymbol{\tau}_{\rm a} + \boldsymbol{\tau}_{\rm z} = -\boldsymbol{m} \times (\nabla_m \varepsilon_{\rm a} - \boldsymbol{H}_{\rm ext}). \tag{13}$$

By using the spherical polar coordinates, the magnetization vector can be written as $\boldsymbol{m} = m\hat{r}_m$ and

$$\nabla_m \varepsilon_{\rm a} = \frac{\partial \varepsilon_{\rm a}}{\partial m}\hat{\boldsymbol{r}}_m + \frac{1}{m}\frac{\partial \varepsilon_{\rm a}}{\partial \theta_m}\hat{\boldsymbol{\theta}}_m + \frac{1}{m\sin\theta_m}\frac{\partial \varepsilon_{\rm a}}{\partial \varphi_m}\hat{\boldsymbol{\varphi}}_m.$$

Hence, the total torque acting on the magnetization vector can be expressed as

$$\boldsymbol{\tau} = -\frac{\partial \varepsilon_{\rm T}}{\partial \theta_m}\hat{\boldsymbol{\varphi}}_m + \frac{1}{\sin\theta_m}\frac{\partial \varepsilon_{\rm T}}{\partial \varphi_m}\hat{\boldsymbol{\theta}}_m, \tag{14}$$

where $\varepsilon_{\rm T} = \varepsilon_{\rm a} + \varepsilon_{\rm zt}$ is the total energy density.

3. Results and discussion

3.1. Easy, intermediate, and hard directions of magnetization from energy consideration

It is known that, in the absence of an external field, the anisotropy of the crystal exerts a torque that rotates the magnetization vector to a direction in which the energy of the crystal is minimum.

For the hexagonal and tetragonal symmetries with $\varepsilon_z = 0$, equations (5) and (6) respectively become

$$\varepsilon_{\rm T} = \alpha\sin^2\theta_m + \gamma\sin^4\theta_m + (\delta + \zeta\cos 6\varphi_m)\sin^6\theta_m, \tag{15}$$

$$\varepsilon_{\rm T} = \alpha\sin^2\theta_m + (\gamma + \delta\cos 4\varphi_m)\sin^4\theta_{\rm m} + (\zeta + \sigma\cos 4\varphi_m)\sin^6\theta_m. \tag{16}$$

It should be noted that only the x and z axes are chosen to lie, respectively, along the a_1 and c axes of both the tetragonal and hexagonal crystals. The y axis, however, in the tetragonal structure is [010], but is [−120] for the hexagonal structure.[51] However from now on, we will use the notation [010] to denote the y axis for either symmetry.

Table 1. Easy and hard magnetization axes for hexagonal and tetragonal crystals, for $\delta = 0$ and $\zeta = 0$, where $E_{010} = E_{100}$.

α	γ	$\alpha+\gamma$	Minimum energy	Easy axis	Hard axis
+	+				
+	−	+	$E_{001} < E_{100}$	⟨001⟩	⟨100⟩
−	+				
+	−				
−	+	−	$E_{100} < E_{001}$	⟨100⟩	⟨001⟩
−	−				
+	$-\alpha$	0	$E_{001} = E_{100}$	⟨100⟩ and ⟨001⟩	...

Table 2. Easy and hard magnetization axes for hexagonal and tetragonal crystals, for $\delta \neq 0$ and $\zeta = 0$, where $E_{010} = E_{100}$.

α	γ	δ	$\alpha+\gamma+\delta$	Minimum energy	Easy axis	Hard axis
+	+	+				
+	+	−				
+	−	+				
−	+	+	+	$E_{001} < E_{100}$	⟨001⟩	⟨100⟩
+	−	−				
−	−	+				
−	+	−				
+	+	−				
+	−	+				
−	+	+				
+	−	−	−	$E_{100} < E_{001}$	⟨100⟩	⟨001⟩
−	−	+				
−	+	−				
−	−	−				

The energies along the main directions [001], [010], and [100] of the hexagonal crystal take the following forms for the systems with four parameters:

$$E_{001} = 0, \tag{17}$$

$$E_{010} = \alpha + \gamma + \delta - \zeta, \tag{18}$$

$$E_{100} = \alpha + \gamma + \delta + \zeta. \tag{19}$$

It is clear from Eqs. (18) and (19) that $E_{010} = E_{100}$ when $\zeta = 0$. The energy analysis, for different signs of the three parameters α, γ and δ, is presented in Table 1 for $\delta = 0$ and in Table 2 for $\delta \neq 0$. With the in-plane parameter ζ included, the situation becomes more complex. Table 3 shows the relative magnetic hardness of the [001], [110], and [100] for different combinations of the parameters α, γ, δ and ζ.

In a similar way, the energies of the tetragonal crystal are given by

$$E_{001} = 0, \tag{20}$$

$$E_{110} = \alpha + \gamma - \delta + \zeta - \sigma, \tag{21}$$

$$E_{100} = E_{010} = \alpha + \gamma + \delta + \zeta + \sigma. \tag{22}$$

Without including the in-plane parameters δ and σ, the energies along the [100], [010], and [110] directions take the same form

$$E_{100} = E_{010} = E_{110} = \alpha + \gamma + \zeta. \tag{23}$$

Our energy analysis is displayed in Tables 1–3, where the relative magnetic easiness/ hardness is assigned to particular crystallographic directions for a given set of the system's parameters.

Table 3. Easy, medium, and hard magnetization axes in hexagonal crystal, with considering four parameters.

α	γ	δ	ζ	E_{100}	E_{010}	Minimum energy	Easy axis	Medium axis	Hard axis
+	+	+	+	+	+	$E_{001} < E_{010} < E_{100}$	⟨001⟩	⟨010⟩	⟨100⟩
−	−	−	−	−	−	$E_{100} < E_{010} < E_{001}$	⟨100⟩	⟨010⟩	⟨001⟩
+	+	+	−	+	+	$E_{001} < E_{100} < E_{010}$	⟨001⟩	⟨100⟩	⟨010⟩
+	+	+	−	−	+	$E_{100} < E_{001} < E_{010}$	⟨100⟩	⟨001⟩	⟨010⟩
+	−	+	+	+	0	$E_{001} = E_{010} < E_{100}$	⟨001⟩ and ⟨010⟩	…	⟨100⟩
−	+	+	+						
+	+	−	−	0	+	$E_{001} = E_{100} < E_{010}$	⟨001⟩ and ⟨100⟩	…	⟨010⟩
+	−	+	−						
−	+	+	−						
+	−	−	+	0	−	$E_{010} < E_{001} = E_{100}$	⟨010⟩	…	⟨001⟩ and ⟨100⟩
−	+	−	+						
−	−	+	+						

3.2. Magnetization curves of uniaxial crystals

3.2.1. Magnetization curves for systems with one and two parameters

The case of a single anisotropy constant, with no peculiar temperature dependence, is straightforward. However an unusual dependence was reported by Millev *et al.*[6] A polynomial interpolation fitting of his data is shown in Fig. 1(a).

We calculated the normalized magnetization at selected reduced temperatures, especially those corresponding to a change in the anisotropy constant sign (e.g. 0.2, 0.4 and 0.5), along and perpendicular to the c axis (Fig. 1(b)). It is clear from Fig. 1(b) that the system is an easy-axis system for positive k, and transforms to an easy-plane system at $T/T_c \geq 0.29$. The simulated normalized magnetization as a function of the reduced temperature is presented in Fig. 1(c). As shown in this figure, the magnetization along the c axis decreases gradually with increasing temperature. This trend is different along the a axis where m increases up to $T/T_c \cong 0.29$ at which it reaches a somewhat round maximum before it saturates at $m \approx 0.7$.

Figure 2(a) shows the magnetization curves for a system described by only two parameters α and γ, where $\alpha/\gamma = -0.5$. The magnetization curves along and perpendicular to the c axis exhibit non-zero magnetization at zero field, namely, $m \approx 0.87$ and 0.49, respectively. This means that the system is an easy-cone with a cone angle of $\sim 29.3^\circ$ off the c axis. This angle is in fair agreement with $\theta_c = 30^\circ$ calculated from the relationship[52] $\theta_c = \sin^{-1}\sqrt{-\alpha/2\gamma}$. Upon changing the sign of α but keeping the same ratio $\alpha/\gamma = 0.5$, the system becomes an easy-axis system. The relative easiness of the c axis at $\varepsilon_z = 0$ is consistent with the energy consideration of Table 1, i.e. $E_{001} < E_{100}$.

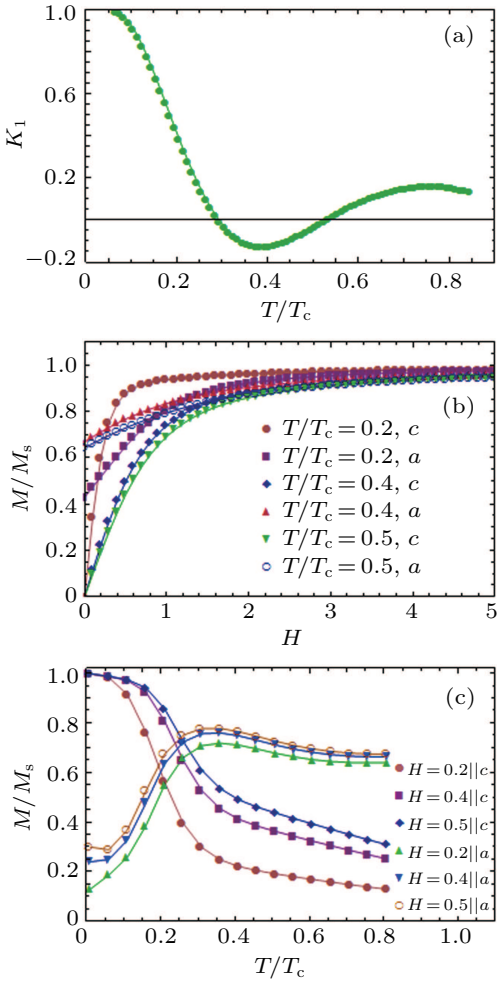


Fig. 1. (color online) (a) Peculiar temperature dependence of anisotropy constant from Ref. [6], (b) field dependence of normalized magnetization at selected reduced temperatures, and (c) temperature dependence of normalized magnetization along and perpendicular to the c axis.

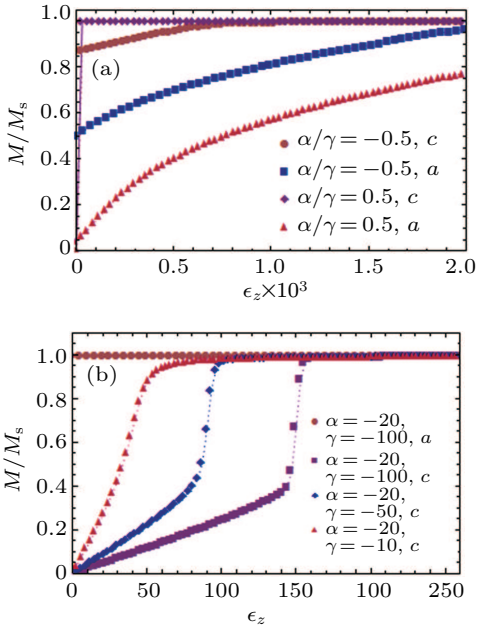


Fig. 2. (color online) Magnetization curve along and perpendicular to the c axis for different values of α and γ.

In case of Fig. 2(b), we have chosen $\alpha = -20$ and set γ to have selected values in the range of -100 to -10. It is clear that for all values of γ, it is easier to magnetize the crystal in the basal plane (i.e., $E_{100} < E_{001}$). In addition, the magnetization curves along the c axis behave in a similar way for different γ values (-100 and -50), where a sudden jump takes place at some ε_z. As the absolute value of γ increases, the critical field, at which the magnetization jumps to saturation, increases. However for $|\gamma| < \alpha$, no such discontinuous jump takes place.

The main features of the magnetization curves shown in Fig. 2 are present in the experimental magnetization curves of easy-plane materials with hexagonal structure, e.g., $Sm_2Fe_{17}N_x$,[28] YCo_4B,[53] and Tb_2Fe_{17}.[54] The $Sm_2Fe_{17}N_x$ system, with different concentrations of interstitial nitrogen in the range $x = 0 - 2.94$, transforms from an easy-plane system for $x = 0$ to an easy-cone one for $x = 0.4$ and then to an easy-axis one for $x \geq 0.55$. These transformations are accompanied with changes in the signs of the anisotropy constants of this system. The magnetization curves of the other two compounds YCo_4B and Tb_2Fe_{17} along the hard direction (c axis) show a discontinuity (interpreted as FOMP) at certain critical fields. In addition, the in-plane anisotropy of the monocrystalline YCo_4B compound is predominant at temperatures $T \leq 110$ K, while for the Tb_2Fe_{17} compound, the anisotropy within the plane is predominant in the whole temperature range. According to the signs and magnitudes of the first and the second anisotropy constants of YCo_4B and Tb_2Fe_{17}, in the absence of an external magnetic field, the magnetocrystalline anisotropy perpendicular to the c axis has negative values in the aforementioned temperature ranges. These results are in fair agreement with the conditions set out in Table 1 that point to the presence of an easy magnetization axis within the basal plane.

3.2.2. Magnetization curves with three parameters and no in-plane anisotropy

For systems with three parameters of different signs and magnitudes (Fig. 3), the hard direction of magnetization is the uniaxial direction (c axis). In addition, the magnetization for different orientations within the basal plane, e.g., [100] and [010], is completely isotropic, which indicates the absence of magnetic anisotropy in this plane. This feature is consistent with the absence of ζ term which influences the in-plane anisotropy (Eq. (5)). We also notice from Fig. 3(a) that the magnetization along the uniaxial direction shows a discontinuity at certain ε_z.

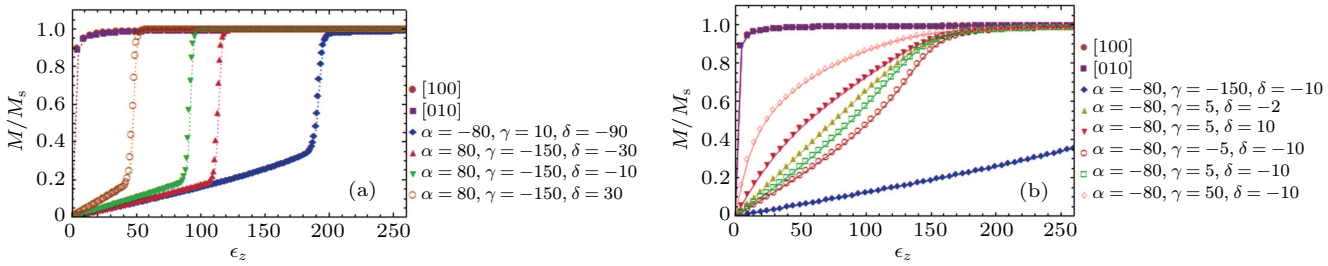


Fig. 3. (color online) Magnetization curves along the [100], [010], and [001] (rest of symbols) directions for (a) different values of α, γ, δ and (b) different values of γ and δ with α equal to -80.

In addition, the magnetization curves along the [001] direction (Fig. 3(b)) are characterized by different curvatures. This behavior of magnetization is attributed not only to the sign of δ but also to the magnitude of γ. For instance, for $\alpha = -80$, $\gamma = 5$, $\delta = 10$ and $\alpha = -80$, $\gamma = 50$, $\delta = -10$, the magnetization has an upward curvature, while for $\alpha = -80$, $\gamma = 5$, $\delta = -10$ and $\alpha = -80$, $\gamma = -5$, $\delta = -10$, the magnetization has a downward curvature. However, for $\alpha = -80$, $\gamma = 5$, $\delta = -2$, the magnetization increases almost linearly up to saturation.

The compounds $(Nd_{1-x}Pr_x)_2Co_{14}B$[29] with $x = 0$–1, $(Nd_{1-x}Pr_x)_2Fe_{14}B$[55] with $x = 0.2$–1, and $Pr_2Fe_{14-x}M_xB$[56]

with M = Si and Ga are selected examples of tetragonal real materials that are described by three anisotropy constants, have no in-plane anisotropy, and exhibited sudden jumps along the c axis.

3.2.3. Magnetization curves with in-plane anisotropy

3.2.3.1. Magnetization curves for a hexagonal crystal with four parameters

Now, we are going to study the effect of including the in-plane parameter ζ in the total energy of a hexagonal system. We divide the discussion in this section into two parts. Firstly, we take all parameters equal to unity in order to understand the effect of their sign changes (Figs. 4 and 5). Secondly, for constant values of α, γ, and δ (Figs. 6 and 7), we study the case of changing the value of ζ, with different signs, on the magnetization. Also, we study the behavior of the magnetization by changing the value of δ and keeping all other parameters as constant with positive or negative signs (Figs. 8 and 9).

Firstly when the three ratios α, γ, δ have positive signs and ζ has a positive or a negative sign (Fig. 4), the crystal is always easier to magnetize along the c axis and harder to magnetize in the basal plane. The sign of δ only has an effect on the hard direction of magnetization. For positive ζ (Fig. 4(a)), [100] is the hardest, while [010] is the hardest for negative ζ (Fig. 4(b)).

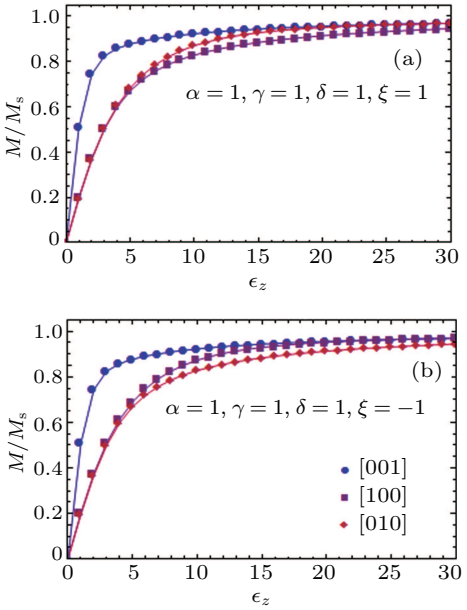


Fig. 4. (color online) Magnetization curves along the [001], [100], and [010] directions for different signs of ζ.

This trend is completely reversed for α, γ, and δ with negative signs and ζ with a positive or a negative sign, as shown in Fig. 5. The c axis becomes the hardest magnetization direction and the basal plane becomes the easy magnetization plane. In the same way, the easiest magnetization direction in the plane depends on the sign of ζ.

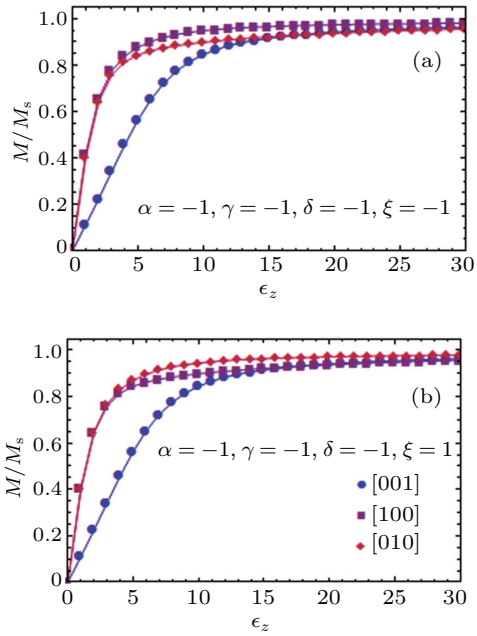


Fig. 5. (color online) Magnetization curves along the [001], [100], and [010] directions for different signs of α, γ, δ, and ζ.

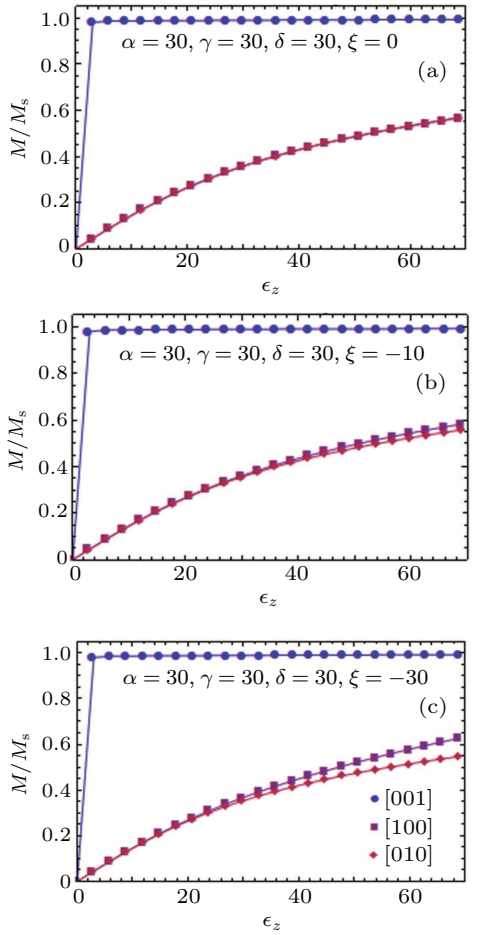


Fig. 6. (color online) Magnetization curves along the [001], [100], and [010] directions for different values of ζ.

Secondly, by taking $\alpha = \gamma = \delta = 30$, and varying the magnitude and sign of ζ in the -80 to 80 range, we find out that the crystal is easily magnetized along the [001] direction and harder to be magnetized along the two other di-

rections [100] and [010], as shown in Figs. 8 and 9. However, for $\zeta = 0$ (Fig. 6(a)), the basal plane is completely isotropic. For lower values of ζ, e.g., ζ in the range of -5 to -30, the in-plane magnetization curves become slightly different from each other for $\varepsilon_z \geq 25$. We display here only two examples for this trend (Figs. 6(b) and 6(c)). As ζ becomes more negative (Figs. 7(a) and 7(b)), the difference between the in-plane directions becomes more evident. A change in the sign of ζ from – to +, keeping all other parameters the same, leads to reversing the in-plane mid-hard and the hard axes, as shown in Figs. 7(b) and 7(c).

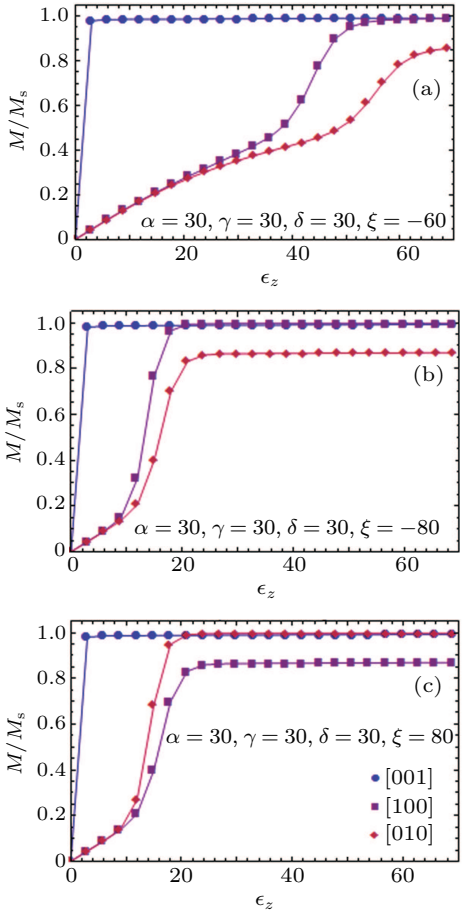


Fig. 7. (color online) Magnetization curves along the [001], [100], and [010] directions for different values of ζ.

The case in Fig. 8 is that of an easy-plane system which exhibits two directions of relative easiness, i.e., [100] and [010], however the magnetic saturation is achieved at $m = 1$ and ~ 0.8 for these directions, respectively. Increasing δ only has an effect on the magnetization along the c axis, where relative easiness of magnetization develops along this direction as δ increases.

In Fig. 9, the opposite behavior of magnetization is observed for α, γ, and ζ with the same values as those in Fig. 8 but with opposite signs, where the c axis becomes the easy magnetization axis. In addition, the anisotropy between the c axis and the plane becomes more dominant when the δ sign changes from + to –.

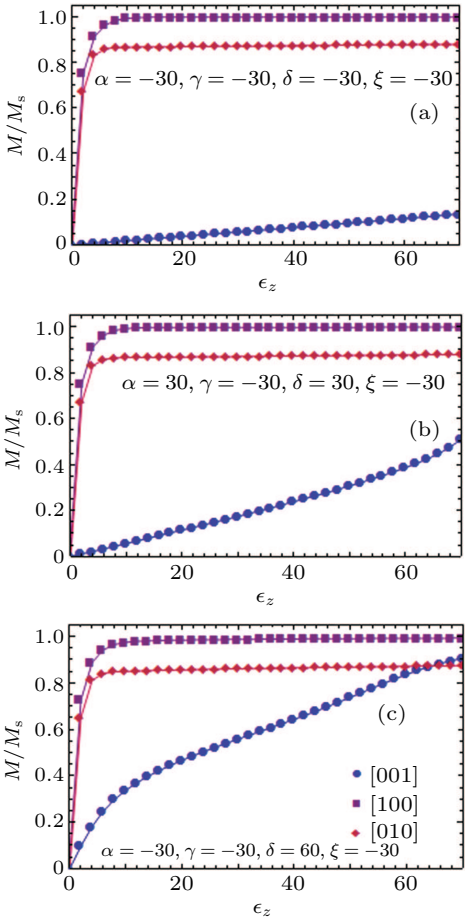


Fig. 8. (color online) Magnetization curves along the [001], [100], and [010] directions for different values of δ.

The isothermal field dependences of magnetization at 4.2 K for Y_2Co_{17} and Gd_2Co_{17} hexagonal compounds have been measured by Matthaei *et al.*[30] They had four anisotropy constants to calculate the magnetization curves for both compounds. Figure 2 in their calculations shows the theoretical beside the experimental curves. They found out that the c axis is the hard axis of magnetization in each compound, with a discontinuity at a critical field of 1.17 T in the Gd_2Co_{17} compound, while no such discontinuity appears for the Y_2Co_{17} compound.

3.2.3.2. Magnetization curves for tetragonal crystal with four and five parameters

The magnetization curves for a tetragonal crystal along the [001], [110] and [100] directions by taking four and five parameters into consideration are shown in Figs. 10 and 11.

Figure 10 displays an interesting case of a magnetization jump that takes place to saturation along the c axis of an easy-plane system. The effect of changing only the sign of δ, in systems otherwise of the same parameters, is changing the easiest in-plane direction from the [110] to the [100] or vice versa, without changing the other features of the magnetization curves (Figs. 10(b) and 10(c)).

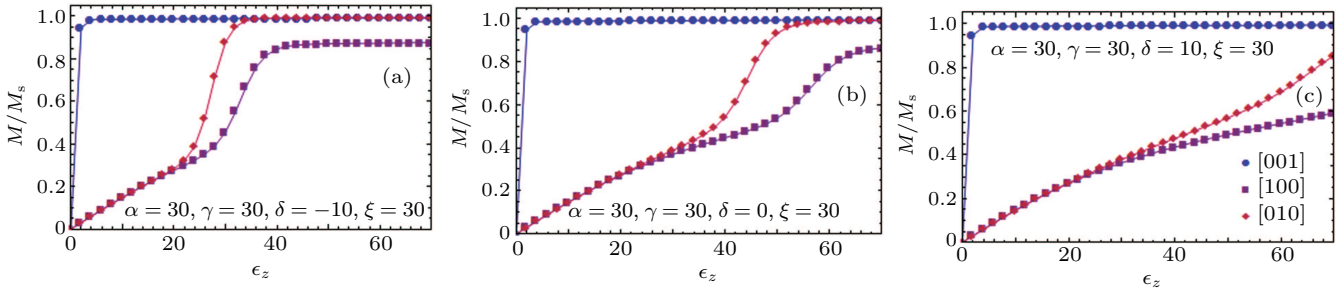


Fig. 9. (color online) Magnetization curves along the [001], [100], and [010] directions for different values of α, γ, δ, and ζ.

From Figs. 10(a) and 11(a), we note that, for $\zeta = 30$ and with including another in-plane parameter $\sigma = -30$, the magnetization along the [001] direction reaches saturation for a relatively small value of ε_z.

For systems with the same values of α, γ, δ and different values of ζ and σ (Figs. 11(b) and 11(c)), the magnetization jump takes place along the [110] direction.

Magnetization curves of different materials, for instance, some rare earth intermetallic compounds $HoFe_{11}Ti$,[57] $Nd_2Fe_{14}B$,[36] $Nd_2Fe_{14}BH$,[37] and $Pr_2Fe_{14}B$,[58,59] display transitions along one or two crystallographic directions within the basal plane. For example, a discontinuity in magnetization only appears along the [100] direction of the $Nd_2Fe_{14}B$ compound. However, for the other three compounds $HoFe_{11}Ti$, $Nd_2Fe_{14}BH$, and $Pr_2Fe_{14}B$, the magnetization shows a discontinuity along both of the [100] and [110] directions.

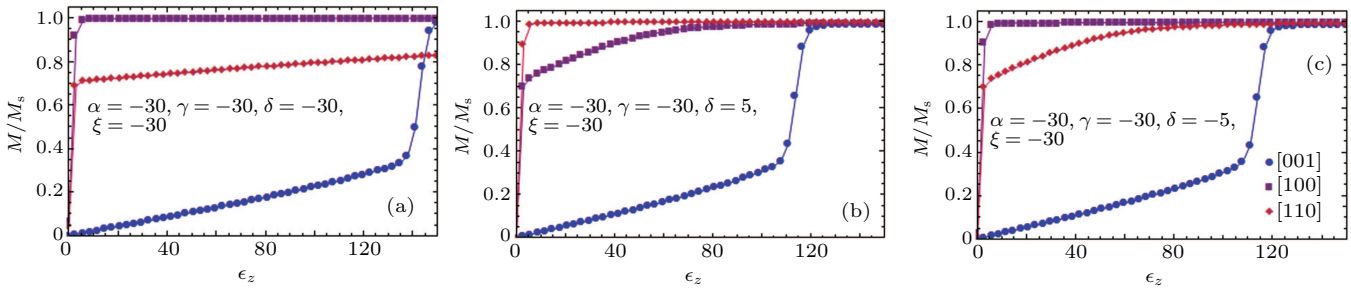


Fig. 10. (color online) Magnetization curves along the [001], [110], and [100] directions for different values of δ.

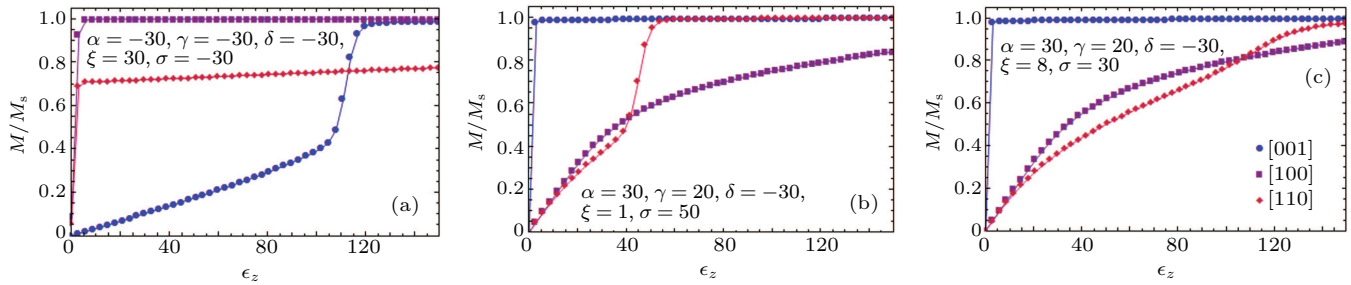


Fig. 11. (color online) Magnetization curves along the [001], [110], and [100] directions for different signs of α, constant δ, and different values of γ, ζ, and σ.

We display in Fig. 12 one example for applying our method to a real material, namely, the $HoFe_{11}Ti$ compound.[57] This compound has a tetragonal structure with an easy-axis along the [001] direction and a hard basal plane. The magnetization within the basal plane displays a discontinuity along each of the [110] and [100] directions for $\varepsilon_z \approx 80$ and 100, which correspond to the critical fields of ~ 18.4 kOe and 23 kOe at 4.2 K as reported by Nikitin *et al.* The anisotropy field ε_z^a along the [100] is about 75 kOe, which is in good agreement with the anisotropy field (~ 75 kOe) reported by Nikitin *et al.*

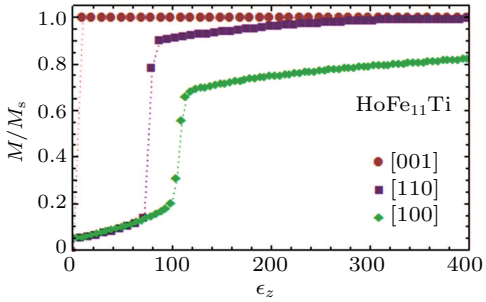


Fig. 12. (color online) Magnetization curves at 4.2 K along the [001], [110], and [100] directions of $HoFe_{11}Ti$.

3.3. Probability landscapes

3.3.1. Probability landscapes for a hexagonal crystal with four parameters

We calculated the probability angular distribution along the main directions of the hexagonal crystal by taking four parameters α, γ, δ, and ζ into consideration. In this section, we give examples for only two different sets of parameters $\alpha=-1$, $\gamma=-1$, $\delta=-1$, $\zeta=1$ (Fig. 13) and $\alpha=-1$, $\gamma=-1$, $\delta=-1$, $\zeta=-1$ (Fig. 14).

Figure 13 shows the probability plots at $\varepsilon_z = 2$ along the [001], [100], and [010] directions. It is clear that all plots display maxima at $\theta_m \sim 1.54$ rad, but at different φ_m, e.g., the angular coordinates of the prominent probability peak along the [010] direction are $\theta_m \sim 1.54$ rad and $\varphi_m \sim 1.5$ rad, which are close to the angular coordinates of the applied field. This probability plot is consistent with the magnetization curve of Fig. 5(b), which indicates that the system is an easy-plane system.

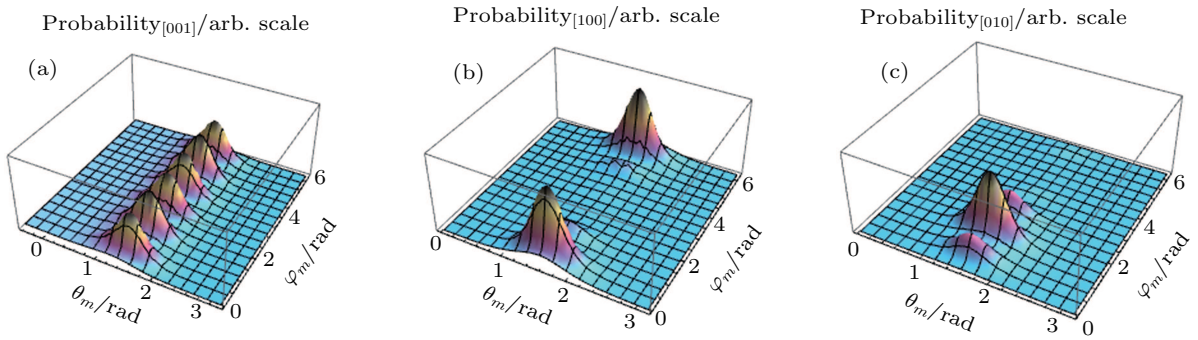


Fig. 13. (color online) Probability landscapes along the three main directions of a hexagonal crystal for $\alpha=-1$, $\gamma=-1$, $\delta=-1$, $\zeta=1$, and $\varepsilon_z=2$.

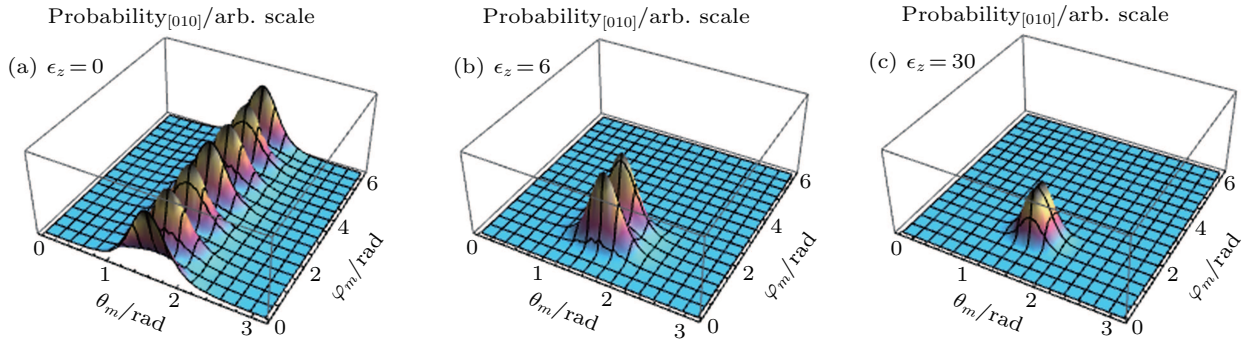


Fig. 14. (color online) Probability landscapes along the [010] direction of a hexagonal crystal for $\alpha=-1$, $\gamma=-1$, $\delta=-1$, $\zeta=-1$, and different ε_z: (a) $\varepsilon_z=0$, (b) $\varepsilon_z=6$, (c) $\varepsilon_z=30$.

The angular dependence of the probability at different ε_z along the [010] direction is presented in Fig. 14 for the same set of parameters as that of Fig. 13 except of $\zeta=-1$. The probability landscape for $\varepsilon_z=0$ (Fig. 14(a)) shows peaks at $\theta_m \sim 1.54$ rad for different φ_m. With increasing ε_z to 6, the probability landscape displays two peaks of an equal intensity at $\varphi_m \sim 1.5$ rad and 2.5 rad (Fig. 14(b)). Furthermore, the number of local maxima decreases as ε_z increases, where the two peaks start to merge at $\varepsilon_z \geq 15$ until they form a single peak at $\varepsilon_z=30$ (Fig. 14(c)).

3.3.2. Probability landscapes of a tetragonal crystal with five parameters

The field-dependence of the angular location of the magnetization vector of an easy-axis tetragonal crystal is shown in Figs. 15 and 16. A value of $\varepsilon_z=20$ along the [001] easy axis orientates the magnetization vector rigidly along its direction with high probability (Fig. 15(a)). Now applying a field with increasing intensity in the basal plane along the [110] direction (Figs. 15(b), 15(c), 16(a), and 16(b)) results in a gradual rotation, against the uniaxial anisotropy, of $\boldsymbol{m}$ along the field direction. Eventually, the most probable orientation is achieved for $\varepsilon_z=55$ at which $\theta_m=\pi/2$ and $\varphi_m=\pi/4$.

3.4. Energy surface with in-plane anisotropy

3.4.1. Energy surface of a hexagonal crystal with four parameters

The 3D plots of energy density, with the same set of parameters as that in Fig. 5(a), for different magnitudes of ε_z along the [010] direction of the hexagonal crystal are presented in Fig. 17. For $\varepsilon_z=1$, the energy surface displays minima along different orientations within the basal plane as demonstrated in Fig. 17(a). As ε_z increases, the energy density along this direction decreases (Fig. 17(b)) until one minimum develops along the [010] direction for $\varepsilon_z=15$ (Fig. 17(c)). This behavior is attributed to the torque exerted by the magnetic field on the magnetization vector. Moreover, the non-isotropic surface of energy (Fig. 17(c)) means that the magnetic saturation is not achieved for $\varepsilon_z=15$, as shown in Fig. 5(a).

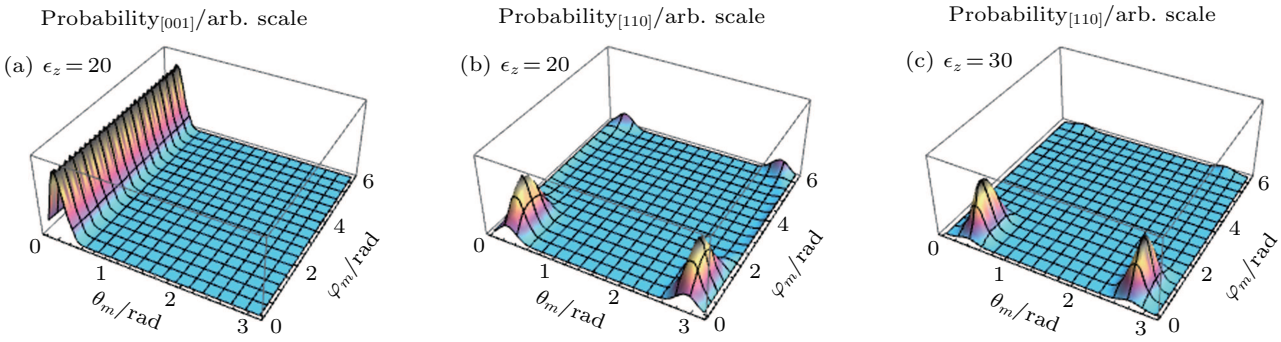


Fig. 15. (color online) Probability landscapes along the [001] and [110] directions of a tetragonal crystal for $\alpha = 30$, $\gamma = 20$, $\delta = -30$, $\zeta = 1$, $\sigma = 50$, and different ε_z: (a) $\varepsilon_z = 20$, (b) $\varepsilon_z = 20$, (c) $\varepsilon_z = 30$.

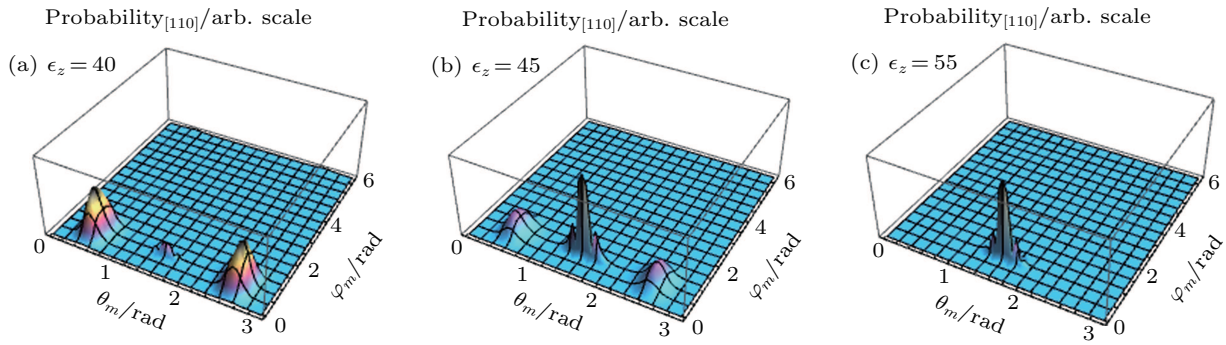


Fig. 16. (color online) Probability landscapes along the [110] direction of a tetragonal crystal for $\alpha = 30$, $\gamma = 20$, $\delta = -30$, $\zeta = 1$, $\sigma = 50$, and different ε_z: (a) $\varepsilon_z = 40$, (b) $\varepsilon_z = 45$, (c) $\varepsilon_z = 55$.

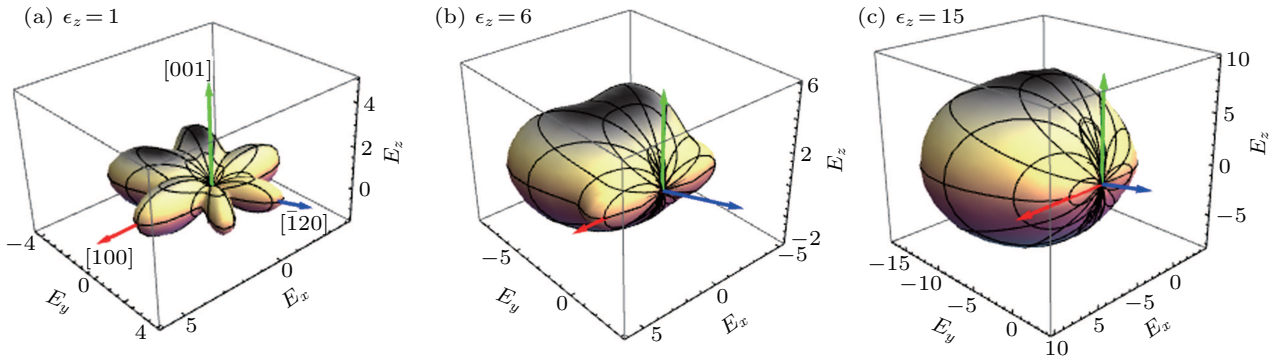


Fig. 17. (color online) 3D energy surfaces for different values of ε_z along the $[\bar{1}20] \equiv [010]$ direction of a hexagonal crystal with the parameters $\alpha = -1$, $\gamma = -1$, $\delta = -1$, $\zeta = -1$, (a) $\varepsilon_z = 1$, (b) $\varepsilon_z = 6$, (c) $\varepsilon_z = 15$.

3.4.2. Energy surface of a tetragonal crystal with five parameters

Figure 18 shows the 3D energy surface plots for an easy-plane tetragonal system, with the same parameters as those in Fig. 11(b). The calculation was performed with ε_z along [001] or [110] direction. For $\varepsilon_z = 20$, the energy surface displays one minimum along the [001] direction, and four minima along different in-plane directions, one of them is located along the [110] direction (Fig. 18(a)). For the same value of $\varepsilon_z = 20$ along the [110] direction (Fig. 18(b)), the energy minimum is located along the [110] direction. However, an $\varepsilon_z = 45$ along the [110] direction is not high enough to cause a single minimum as demonstrated in Fig. 18(c). This is consistent with the magnetization curve along the [110] direction (Fig. 11(b)).

3.5. Energy density and torque landscapes of a tetragonal crystal with five parameters

The energy and torque landscapes for a system whose parameters are those shown in Fig. 16, for constant ε_z applied along the [110] direction, are shown in Fig. 19. It is clear from Fig. 19(a) that the energy density, for $\varepsilon_z = 45$ along the [110] direction, displays minima at the same angles at which the probability maximizes (Fig. 16(b)), namely $\theta_m \sim 0.5$ rad, 1.6 rad, and 2.6 rad for $\varphi_m \sim 0.8$ rad. These angular coordinates are clearly shown in a 2D contour plot in Fig. 2(a). Figures 19(b) and 19(c) display the torque curves along the $\hat{\theta}_m$ and $-\hat{\varphi}_m$ directions, respectively. In addition, the associated contour plots of the torque along the aforementioned directions are shown in Figs. 20(b) and 20(c), respectively.

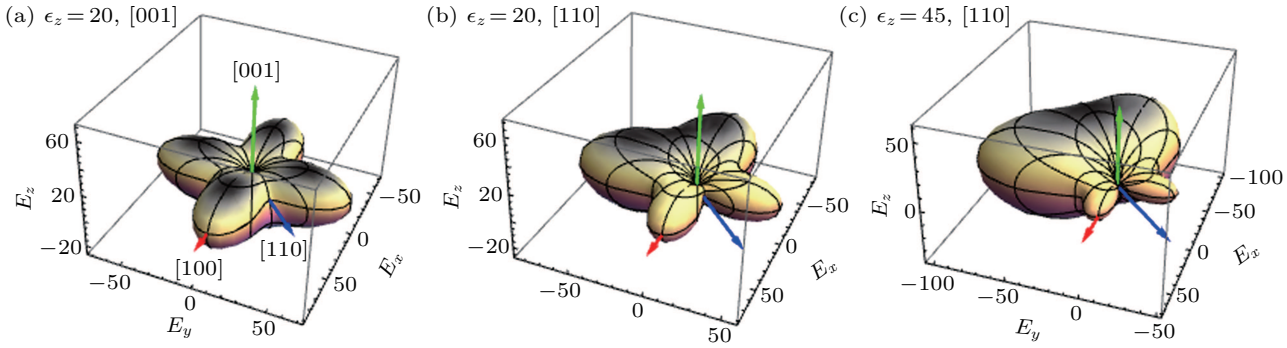


Fig. 18. (color online) 3D energy surfaces of a tetragonal crystal for $\alpha = 30$, $\gamma = 20$, $\delta = -30$, $\zeta = 1$, $\sigma = 50$, and $\varepsilon_z = 20$ along the (a) [001] and (b) [110] directions and (c) $\varepsilon_z = 45$ along [110].

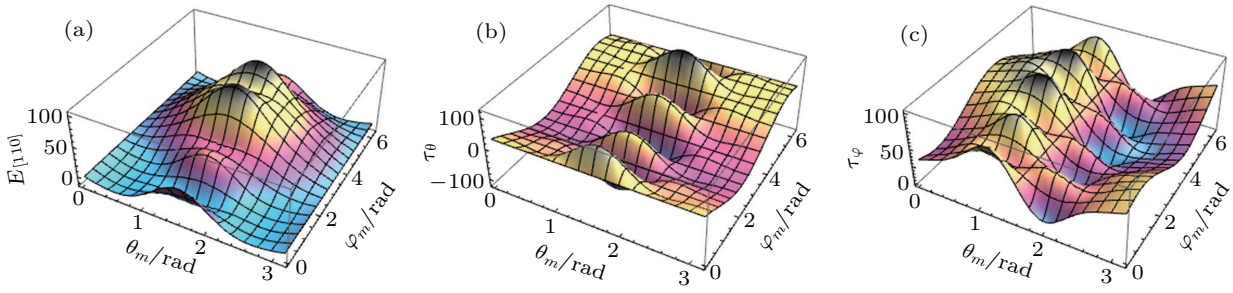


Fig. 19. (color online) (a) Energy and (b), (c) torque landscapes along the [110] direction of a tetragonal crystal for $\alpha = 30$, $\gamma = 20$, $\delta = -30$, $\zeta = 1$, $\sigma = 50$, and $\varepsilon_z = 45$.

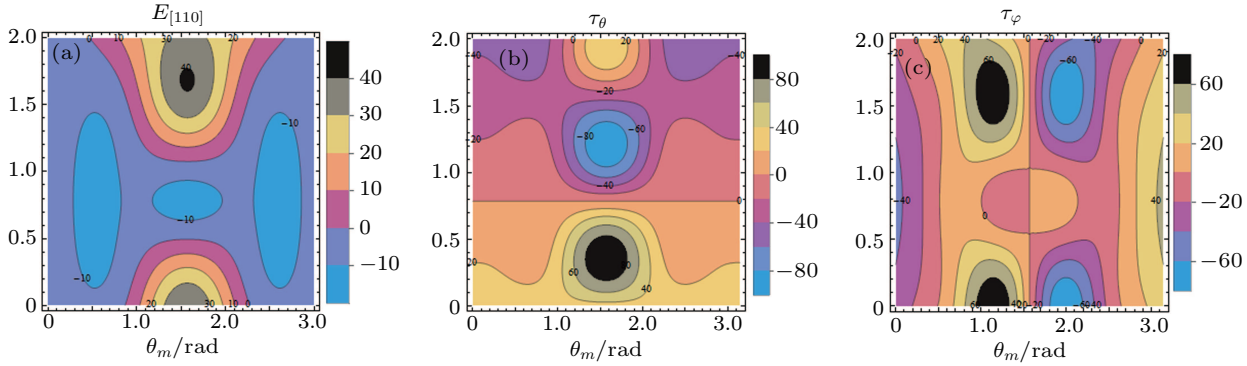


Fig. 20. (color online) Contour plots of (a) energy density and (b), (c) torque for $\varepsilon_z = 45$ along the [110] direction of a tetragonal crystal with the same parameters as those in Fig. 19.

It is well known that the zero-torque corresponds to a minimum as well as a maximum energy. Moreover, the easy- and hard-axes of magnetization could be determined according to the slope sign of the torque curve at $\tau = 0$. As manifested from Fig. 19(c) that the torque curve along the $-\hat{\varphi}_m$ directions has a negative slope at $\theta_m \sim 1.54$ rad for different φ_m. This means that the magnetization vector lies along a direction within the basal plane. The contour plot of the torque along the $\hat{\theta}_m$ direction (Fig. 20(b)) clearly shows that the φ_m at which the torque equals zero is ~ 0.8 rad. The values of $\theta_m \sim 1.54$ rad and $\varphi_m \sim 0.8$ rad correspond to the angular coordinates of the probability maximum (Fig. 16(b)) and the energy minimum (Fig. 20(a)).

4. Conclusion

We have calculated, using the basic laws of classical statistical mechanics, the magnetization curves of hexagonal and tetragonal crystals with up to five anisotropy constants. The energy used in constructing the partition function is the sum of the Zeeman and anisotropy energies. The exchange energy is not considered in the present model which is applicable to single-domain-particle systems or collinear magnetic systems. The system's parameters are normalized to the thermal energy, and the normalized anisotropy parameters are chosen to cover a rather wide range of magnitudes and signs. Such a choice enables us to simulate the magnetization curves of either real material systems e.g., $HoFe_{11}Ti$, or hypothetical systems. The main features of interest of the magnetization curves, e.g., magnetization jumps along [100] or [110], and the

relative magnetic hardiness of the main crystallographic directions in the crystal systems studied have been successfully correlated to the magnetic field dependence of the energy, torque, and probability landscapes.

References

[1] Reif F 1965 *Fundamental of Statistical and Thermal Physics* (New York: McGraw- Hill Inc.) Chap. 6

[2] Getzlaff G 2008 *Fundamentals of Magnetism* (Germany: Springer-Verlag) Chap. 7

[3] Cullity B D and Graham C D 2009 *Introduction to Magnetic Materials* (2nd Edn.) (New Jersey: Wiley IEEE press) Chap. 7

[4] Oliveria de Jesus J C and Kleemann W 1997 *J. Magn. Magn. Mater.* **169** 159

[5] AiMin W and Hua P 2009 *Sci. China Ser. G Phys. Mech. Astron.* **52** 978

[6] Asti G and Bolzoni F 1980 *J. Magn. Magn. Mater.* **20** 29

[7] Kuzmin M D and Tishin A M 2008 *Handbook of Magnetic Materials* (Buschow K H J, Ed.) (North-Holland: Elsevier) Vol. **17** Chap. 3

[8] Millev Y and Fahnle M 1996 *IEEE Transactions on Magnetics* **32** 4743

[9] Millev Y and Fahnle M 1995 *Phys. Rev. B* **52** 4336

[10] Kaczmarek W A and Pietrzak J 1986 *Phys. Stat. Sol. (a)* **98** K43

[11] Qian J F, Liu E K, Feng L, Zhu W, Li G J, Wang W H, Wu G H, Du Z W and Fu X 2011 *App. Phys. Lett.* **99** 252504

[12] Opahle I, Richter M, Kuzmin M D, Nitzsche U, Koepernik K and Schramm L 2005 *J. Magn. Magn. Mater.* **290–291** 374

[13] Bozorth R M 1936 *Phys Rev* **50** 1076

[14] Johnson Jr C E and Brown Jr W F 1961 *J. Appl. Phys.* **32** 243s

[15] Kim Y B and Han-min J 1998 *Journal of Magnetics* **3** 74

[16] Mushnikov N V, Korolyov A V, Gaviko V S, Raevski Ye I and Pareti L 1991 *J. Appl. Phys.* **70** 2768

[17] Hatta S and Chikazumi S 1977 *J. Phys. Soc. Jpn.* **43** 822

[18] Mészáros I 2011 *J. Phys: Conf. Ser.* **268** 012020

[19] Zhdanova O V, Lyakhova M B and Pastushenkov Y U G 2013 *The Physics of Metals and Metallography* **114** 553

[20] Bolzoni F and Pirini M F 1990 *J. Appl. Phys.* **68** 2315

[21] Herbst J F 1991 *Rev. Mod. Phys.* **63** 819

[22] Yamada M, Kato H, Yamamoto H and Nakagawa Y 1988 *Phys. Rev. B* **38** 620

[23] Cadogan J M, Gavigan J P, Givord D and Li H S 1988 *J. Phys. F: Met. Phys.* **18** 779

[24] Kato H, Yamada M, Kido G, Nakagawa Y, Hirosawa S and Sagawa M 1988 *J. Phys. Colloq. C8* **49** 575

[25] Su G 2013 *Advanced Materials Research* **818** 72

[26] Geshev J, Pereira L G, Schmidt J E and Mikhov M 2001 *J. App. Phys.* **90** 6243

[27] Millev Y T, Oepen H P and Kirschner J 1999 *J. Appl. Phys. D* **32** 2599

[28] Katter M, Wecker J, Kuhrt C, Schultz L and Grossinger R 1992 *J. Magn. Magn. Mater* **117** 419

[29] Sun X K, Zhao Z, Wang Q, Zhong X, Zhang Z and Chuang Y C 1991 *J. Appl. Phys.* **69** 5548

[30] Matthaei B, Franse J, Sinnema S and Radwnski R 1988 *Journal de Physique Colloque C8* **49** 533

[31] Bedanta S and Kleemann W 2009 *J. Phys. D: Appl. Phys.* **42** 013001

[32] R Betancourt J I 2002 *Rev. Mex. Fis.* **48** 283

[33] Kim Y B and Han-min J 2000 *J. Magn. Magn. Mater.* **222** 39

[34] Tang N, Kou X C, de Boer F R, Buschow K H J, Wang J L and Yang F 1999 *J. Phys.: Condens. Matter* **11** 5313

[35] Bozorth R M 1937 *J. Appl. Phys.* **8** 575

[36] Bolzoni F, Moze M and Pareti L 1987 *J. Appl. Phys.* **62** 615

[37] Mushnikov N V, Terentev P B and Rosenfeld E V 2007 *Phys. Met. Metallogr.* **103** 39

[38] Yu M H, Zhang Z D and Zhao T 1999 *J. Magn. Magn. Mater.* **195** 327

[39] Kim Y B and Han-min J 1998 *J. Magn. Magn. Mater.* **182** 55

[40] Asti G and Bolzoni F 1985 *J. Appl. Phys.* **58** 1924

[41] Terent'ev P B, Mushnikov N V, Gaviko V S, Shreder L A and Rosenfeld E V 2008 *J. Magn. Magn. Mater.* **320** 836

[42] Kouvel J S 1957 *J. Appl. Phys.* **28** 704

[43] Yu M H, Zhang Z D, de Boer F R, Bruck E and Buschow K H J 2002 *Phys. Rev. B* **65** 104414

[44] Westerstrand B 1975 *Phys. Scr.* **11** 383

[45] Verhoef R, Wang Q and Franse J J M 1992 *Physica B* **177** 211

[46] Kim M J, Kim Y B and Kim T K 2000 *J. Magn. Magn. Mater.* **217** 106

[47] Andreev A V, Deryagin A V, Kudrevatykh N V, Mushnikov N V, Reimer A V and Terentev S V 1986 *Sov. Phys. JETP* **63** 608

[48] Kim Y B, Kim M J, Han-min J and Kim T K 1999 *J. Magn. Magn. Mater.* **191** 133

[49] Tereshina I S, Nikitin S A, Ivanova T I and Skokov K P 1998 *J. Alloys Compd.* **275–277** 625

[50] Kamra A, Schreier M, Huebl H and Goennenwein S T B 2014 *Phys. Rev. B* **89** 184406

[51] Cullity B D 1978 *Elements of X-ray Diffraction* (2nd Edn.) (London: Addison-Wesley company) Chap 2

[52] Skomski R 2008 *Simple Models of Magnetism* (Newyork: Oxford University Press) Chap 3

[53] Thang C V, Brommer P E, Thuy N P and Franse J J M 1997 *J. Magn. Magn. Mater.* **171** 237

[54] Tereshina E A, Drulis H, Skourski Y and Tereshina I S 2013 *Phys. Rev. B* **87** 214425

[55] Huang Y K, Wu C H, Chuang Y C, Yang F M and de Boer F R 1987 *Journal of the Less-Common Metals* **132** 317

[56] Zhong X P, Wang Q, Wu C H, Yang F M, Tang N, Buschow K H J and de Boer F R 1991 *Joumal of the Less-Common Metals* **171** 213

[57] Nikitin S A, Tereshina I S, Skourski Yu V, Pankratov N Yu, Skokov K P, Zubenko V V and Telegina I V 2001 *Physics of the Solid State* **43** 290

[58] Verhoef R, Franse J J M, Menovsky A A, Radwanski R J, Ji Q, Yang Fu M, Li H S and Gavigan J P 1988 *Journal de Physique Colloque C8* **49** 565

[59] Hiroyoshi H, Kato H, Yamada M, Saito N, Nakagawa Y, Hirosawa S and Sagawa M 1987 *Solid State Commun* **62** 475